water

MDPI

Article

Enhanced Photocatalytic Degradation of the Antidepressant Sertraline in Aqueous Solutions by Zinc Oxide Nanoparticles

Zeinhom H. Mohamed [1], Yasser M. Riyad [2,*], Hassan A. Hendawy [3] and Hassan M. H. Abdelbary [4]

[1] Department of Chemistry, Faculty of Science, Jazan University, Jazan P.O. Box 82817, Saudi Arabia; zmohamed@jazanu.edu.sa
[2] Department of Chemistry, Faculty of Science, Islamic University of Madinah, P.O. Box 170, Madinah 42351, Saudi Arabia
[3] The National Organization for Drug Control and Research, 6 Abu Hazem St., Pyramids Ave., Giza 12655, Egypt; dhassanhendawy@gmail.com
[4] Department of Chemistry, Faculty of Science, Al-Azhar University, Nasr City, Cairo 11884, Egypt; hassanambdelbary@azhar.edu.eg
* Correspondence: yasser.riyad@iu.edu.sa

Abstract: Antidepressants are one of the main pollutants in the aquatic environment. They are being widely studied due to their widespread use, possible health effects, and partial removal from wastewater treatment plants by conventional methods. Photocatalysis is an effective and ecologically beneficial method in wastewater treatment. In the present study, the photocatalytic degradation of sertraline hydrochloride (SERT) in water using nano-sized zinc oxide (ZnO-NPs) was investigated. The ZnO-NPs were synthesized from zinc gluconate as a precursor by the sol–gel method. The crystal structure, morphology, surface charge, and textural properties were characterized by X-ray diffraction, scanning electron microscopy, energy-dispersive X-ray analyses, transmission electron microscopy, Fourier-transform infrared spectroscopy, zeta potential, and N_2 adsorption–desorption measurements. The removal of SERT in water was explored by different processes: H_2O_2/UV, ZnO-NPs/H_2O_2/UV, and ZnO-NPs/UV. Our results indicate that the combination of both UV illumination and the ZnO-NP as a catalyst was necessary for the efficient degradation of the drug. Nearly complete removal of SERT (98.7%) was achieved in 30 min with the ZnO-NPs/UV process at room temperature. The photodegradation of SERT follows first-order kinetics with a rate constant of 0.0678 min^{-1}. The results reveal that SERT degradation with ZnO-NPs/UV is pH-dependent, as the maximum drug removal was achieved at pH 11. Initial drug concentration, catalyst dose, and hydrogen peroxide concentration were also crucial in the removal of SERT. Our findings indicate that the high specific surface area and porous structure of ZnO-NP enhance its photocatalytic performance toward photodegradation of SERT, i.e., ZnO-NP is an efficient nanophotocatalyst for the degradation of SERT under UV irradiation.

Keywords: water treatment; pharmaceuticals; sertraline; photocatalysis; zinc oxide nanoparticle

Citation: Mohamed, Z.H.; Riyad, Y.M.; Hendawy, H.A.; Abdelbary, H.M.H. Enhanced Photocatalytic Degradation of the Antidepressant Sertraline in Aqueous Solutions by Zinc Oxide Nanoparticles. *Water* **2023**, *15*, 2074. https://doi.org/10.3390/w15112074

Academic Editor: Alexandre T. Paulino

Received: 21 April 2023
Revised: 20 May 2023
Accepted: 25 May 2023
Published: 30 May 2023

1. Introduction

Environmental pollution resulting from pharmaceuticals is a global problem that has received considerable attention recently due to their possible health effects, widespread nature, and difficult degradation through conventional techniques [1]. These pollutants are transferred mainly to the aquatic environment through effluents from wastewater plants and hospitals [2]. The presence of antidepressant pharmaceuticals in wastewater has received particular attention among the various classes of emerging contaminants due to their widespread use, heavy consumption, and toxicological effects [3,4]. These compounds can help relieve symptoms of depression, anxiety disorders, seasonal affective disorder, and dysthymia.

Over the last decades, the concentration and effects of pharmaceutical compounds, including psychiatric drugs, in the aquatic environment have been assessed [5]. Sertraline hydrochloride (SERT), one of the pharmaceutical compounds, is primarily used to treat clinical depression in adult outpatients as well as obsessive–compulsive, panic, and social anxiety disorders in both adults and children [6]. As a result, SERT has become one of the most commonly detected pharmaceuticals in surface water and wastewater treatment plant effluents [7]. Because of the low removal rates of SERT from wastewater, it is necessary to search for alternative and more effective treatment methods.

Advanced oxidation processes are effective and ecologically beneficial approaches employed in wastewater treatment. Among these methods is photocatalysis, characterized by a simple instrumental procedure, an easily controlled process, non-selective oxidation, being cost-effective, and bringing about a complete degradation of pharmaceutical pollutants [8]. The decomposition of pollutants by photocatalysts occurs by the electron–hole pairs generated via either visible or UV irradiation according to the band energy gap of photocatalysts [9,10]. The most commonly used and effective photocatalysts in wastewater treatment include TiO_2, ZnO, and CdS [10,11]. Among these photocatalysts, ZnO is mostly used in wastewater treatment due to its wide energy band gap of 3.37 eV and its high excitation binding energy of 60 meV (at an ambient temperature of 300 K) [8,12].

One-dimensional nanorods, in comparison with nanoparticles, have a high specific surface area, a high capability for charge transfer, and carrier mobility throughout the photocatalyst [13–15]. Furthermore, the nanorod-like structure provides a high light absorption capacity, large charge separation, and high adsorption of pollutants [15]. Consequently, the ZnO nanorods structure can be more beneficial to the light-assisted photocatalytic degradation of different water pollutants, such as dyes and pharmaceuticals. Compared to nanorods and nanoparticles, two-dimensional nanomaterials provide enhanced physical and chemical functionality owing to their unique structure properties, high surface-to-volume ratios, and surface charges. Two-dimensional nanomaterials were recently used in the development of many water treatment systems with remarkable adsorptive and photocatalytic degradation [16]. Two-dimensional nanomaterials includes a broad spectrum of nanomaterials, including polymer-based materials, metal nanosheets, graphene-based materials, transition metal oxides/dichalcogenides, etc.

The aim of the present work is to synthesize ZnO-NPs using the sol–gel chemical method and to investigate the efficiency of the synthesized nanoparticles for degrading SERT from the aquatic environment under different processes: H_2O_2/UV, ZnO-NPs/H_2O_2/UV, and ZnO-NPs/UV. Moreover, the optimalconditions for the photocatalytic degradation of SERT in the presence of ZnO-NPs were identified. These include the effect of pH, initial drug concentration, amount of catalyst, and hydrogen peroxide concentration. The kinetics of the photocatalytic degradation process were investigated using the zero-order, first-order, and second-order kinetic models. Furthermore, monitoring of the percentage of chemical oxygen demand (COD) during the photocatalytic degradation process was imperative to this study as it was an essential indicator for SERT mineralization, affirming the effectiveness of the water treatment process. We show here that ZnO-NPs could be used effectively as a photocatalyst for the degradation and mineralization of SERT in water.

2. Materials and Methods

2.1. Chemicals

SERT((1S)-cis-4-(3,4-dichlorophenyl)-1,2,3,4-tetrahydro-N-methyl-1-naphthalenamine) was purchased from El-Nasr Pharmaceutical Company, Cairo, Egypt, while zinc gluconate was obtained from EPICO Pharmaceutical Company, Karmouz, Egypt, and zinc oxide bulk was purchased from Sigma-Aldrich (St. Louis, MO, USA) (purity 99.9%, surface area: 4.83 $m^2\ g^{-1}$, and average pore size < 5 micron). Figure 1 represents the chemical structure of SERT. Hydrogen peroxide (30% w/w), sodium hydroxide, ammonia solution, ferrous ammonium sulfate, ferroin indicator, mercury (II) sulfate, and potassium dichromate were

purchased from BDH Company. All other reagents were analytical-grade and used as received. All solutions were prepared with deionized (DI) water.

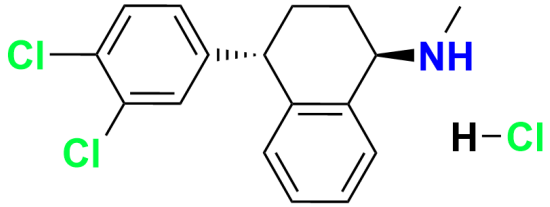

Figure 1. Chemical structure of Sertraline hydrochloride (SERT).

2.2. Synthesis and Characterization of Nano-Sized Zinc Oxide

2.2.1. Synthesis

ZnO-NPs were synthesized via the sol–gel method by dissolving 2 g of zinc gluconate in 100 mL deionized water. The solution was sonicated for 10 min to completely dissolve the zinc gluconate. Ammonia solution was slowly dropped into zinc gluconate solution with continuous stirring, then the resultant precipitate was collected by filtration under vacuum and rinsed four times with deionized water and ethanol. The precipitate was dried at 90 °C, then calcinated at 600 °C for 3 h in the muffle furnace to give ZnO-NPs as shown in the following Equations:

$$Zn(C_6H_{11}O_7)_{2(aq)} + 2\,NH_4OH_{(aq)} \rightarrow Zn(OH)_{2(s)} \downarrow + 2C_6H_{11}O_7NH_{4(aq)} \quad (1)$$

$$Zn(OH)_{2(aq)} \downarrow + 2OH^- \rightarrow ZnO_2^{-2} + 2H_2O \quad (2)$$

$$ZnO_2{}^{-2} + H_2O \rightarrow ZnO \downarrow + 2OH^- \quad (3)$$

2.2.2. ZnO-NPs Characterization

FTIR spectroscopy of zinc gluconate, ZnO-NPs, and bulk ZnO was conducted in the 400–4000 cm^{-1} region using a Perkin Elmer spectrometer (FTIR, Perkin Elmer, Hamburg, Germany). The FTIR spectra were processed by Prestige software (IR solution, version 1.50). A cylindrical holder was used to press sample powders (200 mg, 1 wt.% in KBr) until a disk (13 mm diameter, 2 mm thickness) was obtained.

X-ray diffraction (XRD) was used to investigate the structural and crystalline properties of the synthesized ZnO-NPs particles in the2θ range of 10–60° by using a Bruker AXS -D8 advanced diffractometer system (Bruker Co., Berlin, Germany), using the manual DIFFRC Plus EVA 2001 method at 25 °C. Based on the width of the XRD peaks, the Scherrer formula was used to determine the ctystalline domain size with the assumption that they are free from non-uniform strains; the formula:

$$D = 0.94\lambda/\beta Cos\theta \quad (4)$$

where D is the average crystallite domain size perpendicular to the reflecting planes, λ is the X-ray wavelength, β is the full width at half maximum (FWHM), and θ is the diffraction angle.

A scanning electron microscope (SEM), model Quanta 250 FEG (Field Emission Gun) with an EDX unit (energy dispersive X-ray analyses), at an accelerating voltage of 30 KV, was used to observe the morphology and the elemental analysis of the ZnO-NPs. The prepared sample was kept on a SEM stub using double-sided adhesive tape at 50 mA for 6 min through a sputter. Afterwards, the stub containing the sample was placed in the SEM chamber. At an acceleration voltage of 20 kV, the photomicrograph was taken.

Moreover, a transmission electron microscope (TEM), model JEM-2100 Plus, was used to conduct characterization of ZnO-NPs. The TEM samples were prepared by sonicating the produced powder after mixing it with ethanol. Thereafter, a small drop of the sample

was applied to the staining mat. The sample was coated with a copper grid, then removed and air-dried. Then, the sample was analyzed at an accelerating voltage of 80 kV.

Surface charge of ZnO-NPs was measured by determining zeta potential using the Malvern zeta-sizer nanoseries (UK). Furthermore, the surface area and porosity of ZnO-NPs was calculated by nitrogen adsorption–desorption analysis at 77 K using a Micromeritics ASAP 2010 instrument. The specific surface area of the sample was determined by the BET method and the pore size and pore volume distribution was assessed by the Barrett–Joyner–Halenda (BJH) method.

2.3. Photoreactor and Actinometry

Photoreactions were carried out in an ACE glass photoreactor comprised of a quartz tube surrounded with a water-cooling jacket and immersed in a Pyrex cylinder as a solution container. The container had inlets for feeding reactants and ports for measuring temperature and withdrawing samples. The UV irradiation source was a 20 W low-pressure mercury vapor lamp (maximum emission at 254 nm). The incident photonic flux was measured by the photolysis of ferrioxalate (I_o = 1.46 $\times 10^{-6}$ Ein./L min).

2.4. Photocatalytic Degradation Procedure

The photoreactor was operated with an initial working volume of 100 mL. Solutions were prepared by dissolving the necessary quantity of the drug and H_2O_2 in distilled water and fed into the photoreactor. The aqueous solutions were magnetically stirred, and the temperature was maintained at 25 ± 2 °C by water circulation through an internal cooling tube. The pH of the solution was measured by a HANA pH-Meter and adjusted by using Britton–Robinson (BR) buffer solutions. The lamp initiated the reaction after 5 min of premixing and samples were taken at regular intervals.

Additionally, 0.02 g of the synthesized photocatalyst zinc oxide was added to 100 mL of 0.1 mM SERT aqueous solution at 25 °C with natural pH (pH 7.3). Before UV illumination, the suspension was magnetically stirred in the dark for 10 min to disperse the catalyst. The reactor was then irradiated with UV light emitted by 20 W UV light lamp (λ = 254 nm). At defined intervals, analytical samples were taken from the reaction suspensions during the reaction and then were centrifuged to remove the suspended particulates. The concentration of the SERT solution was determined by measuring the absorbance with bromophenol blue (BPB) using a UV-Vis spectrophotometer double-beam Perkin Elmer (UV-Vis 170) [17].

2.5. Analytical Procedures

Solutions withdrawn from the photoreactor were used to analyze the degradation % and chemical oxygen demand (COD). The concentration of the SERT solution was determined by measuring the absorbance with bromophenol blue (BPB) using a Schimadzu UV–160A spectrophotometer [17]. Chemical oxygen demand (COD) was determined using the closed reflux method to oxidize samples with a known excess of $K_2Cr_2O_7$ in 50% H_2SO_4 solution [18]. A standard ferrous ammonium sulfate solution was used to titrate excess $K_2Cr_2O_7$. The removal % of SERT was calculated according to Equation (5):

$$\text{Drug \% Removal} = \frac{C_o - C_t}{C_o} \times 100 \quad (5)$$

where C_o is the initial SERT drug concentration and C_t is the drug concentration at time t.

2.6. Kinetic Analysis

The kinetics for the whole process of SERT photocatalytic degradation by ZnO-NPs was described by using three kinetic models, as shown in Equations (6)–(8) for the zero-order, first-order, and second order, respectively.

$$C_o - C_t = kt, \quad (6)$$

$$\ln\left(\frac{C_t}{C_o}\right) = -kt \quad (7)$$

$$\left(\frac{1}{C_t} - \frac{1}{C_o}\right) = kt \quad (8)$$

where C_o is the initial drug concentration, C_t is the drug concentration at any time (t), and k is the rate constant of the photocatalytic degradation process.

3. Results and Discussion

3.1. Characterization of ZnO-NPs

The FTIR spectra of zinc gluconate, pure bulk ZnO, and prepared ZnO-NPs are shown in Figure 2a. The FTIR spectrum of zinc gluconate displays a broad band at 3400 cm^{-1}, which could be assigned to a hydroxyl group (O-H) stretching of gluconate anions [19]. However, for the Bulk ZnO and ZnO-NPs, the peak at 3400 cm^{-1} could be attributed to the water of hydration present in the solution during the synthesis process. Furthermore, all characteristic bands of the gluconate skeleton appeared in the finger print region from 1200 cm^{-1} to 400 cm^{-1}, together with the C=O stretching of carboxylate group appearing at 1750 cm^{-1} [20]. All bands of the gluconate anion disappeared in the case of bulk ZnO and ZnO-NPs. Indeed, a new significant band appearing at 440 cm^{-1} and 450 cm^{-1} for the pure bulk and nanoparticles of ZnO, respectively, which could be associated with the Zn–O stretching mode of the ZnO [21,22]. The band at 450 cm^{-1} recorded for the ZnO-NPs exhibits a red shift compared to pure bulk ZnO. This behavior is due to the small particle size and morphology of prepared ZnO-NPs, which may affect the FTIR spectrum [23,24].

The XRD analysis was used to identify the sample's shape and crystalline size. Figure 2b indicates the XRD pattern of the synthesized ZnO-NPs calcined at 600 °C. As shown from the spectra, there are characteristic peaks at 2θ values of 31.7°, 34.3°, 36.2°, 47.6°, and 56.6° for reflections at the 100, 002, 101, 102, and 110 planes, respectively. All peaks could be indexed as the zinc oxide wurtzite structure (JCPDS Data Card No: 36-1451). These peaks can be indexed to ZnO's hexagonal zincite-type crystallite [25]. Moreover, the Scherrer equation was used to determine the crystalline size of the ZnO-NPs of 53.88 nm.

Figure 2c shows the EDX spectrum of the ZnO-NPs, which confirms the presence of zinc and oxygen signals in the synthesized nanomaterial. The elemental analysis of the synthesized ZnO-NP yielded 82.49% of zinc, 11.65% of oxygen, and 5.84% of carbon. Our results agree with the data published in the literature [26].

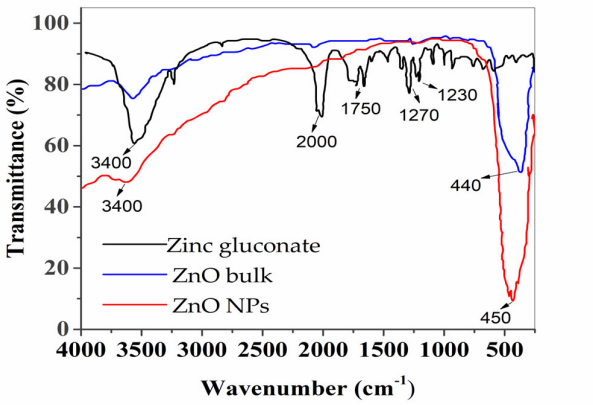

(**a**)

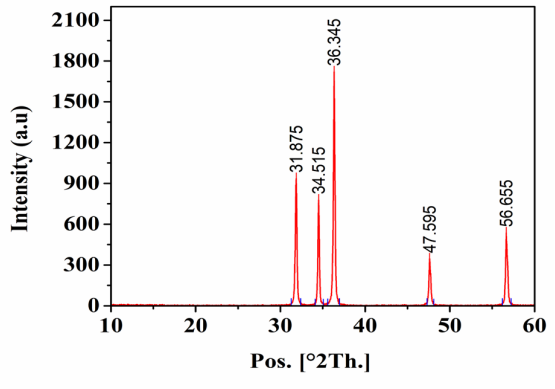

(**b**)

Figure 2. *Cont.*

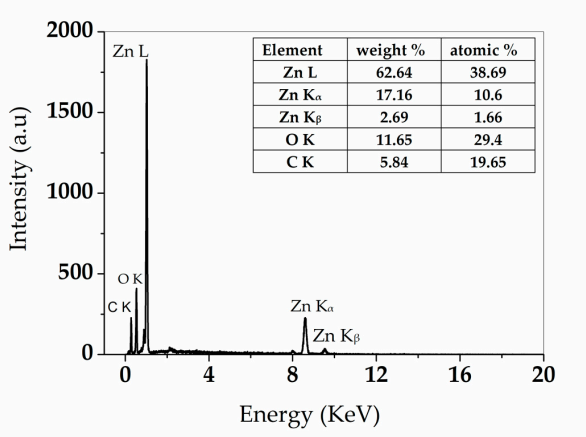

(**c**) (**d**)

Figure 2. (**a**) FTIR spectra obtained from zinc gluconate and the bulk ZnO and ZnO-NPs; (**b**) XRD pattern, (**c**) EDX, and (**d**) zeta potential of the synthesized ZnO-NPs.

Figure 3 indicates the typical scanning electron microscope (SEM) image of the synthesized ZnO-NPs. It is evident from the image that the morphology of ZnO is a nearly spherical shape. The SEM image of ZnO-NPs demonstrates the spherical shape and highly porous structure of ZnO-NPs. The presence of aggregates in the SEM image is due to the accumulation of ZnO-NP crystals with a dense structure during the calcination process [27].

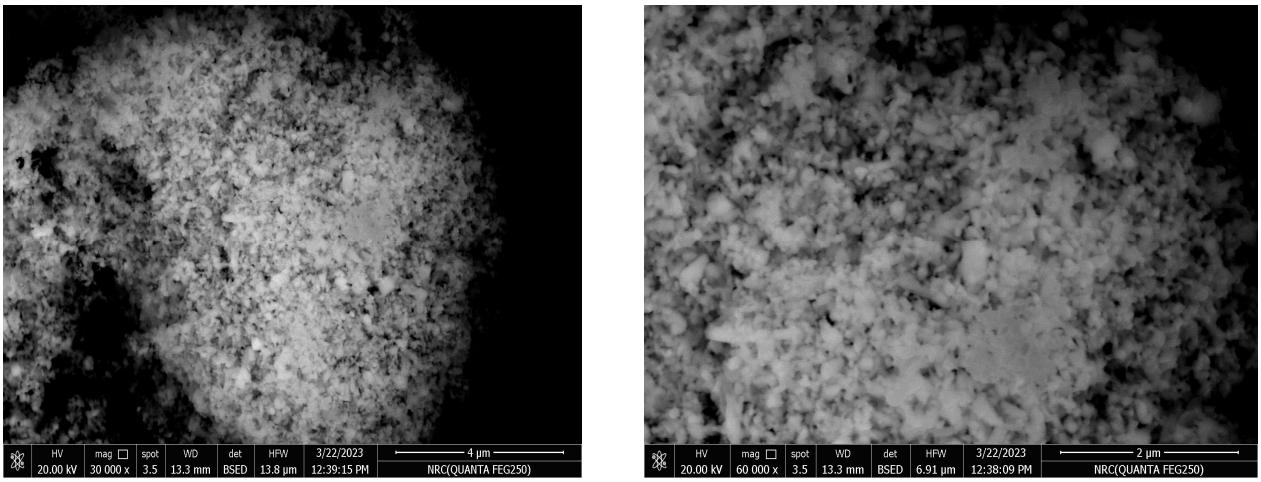

(**a**) (**b**)

Figure 3. Scanning electron microscopy images of the synthesized ZnO-NPs at scale (**a**) 4 µm and (**b**) 2 µm.

TEM was used to observe further the ZnO-NPs' morphology (see Figure 4). There is a tendency for the ZnO particles to form subtle clusters of different shapes, including tetrahedral, rod-shaped, and cube-shaped particles, as well as a certain percentage of spherically shaped particles. Particle sizes ranged from 22 to 76 nm, with an average crystal size of 33.6 nm. Moreover, the structure of ZnO-NPs depicts a nanorod-like structure (~200 nm), along with nanosized particles that can be obtained at high temperature (≥500 °C) [28].

Zeta potential was used to measure the surface charges of ZnO-NPs. Zeta potential is a physical characteristic of particles in suspension, representing electrostatic repulsion or attraction between ZnO-NPs and SERT. The electrostatic attraction may play a role in the removal of SERT based on the pH of the aqueous solution, as will be discussed later. Figure 2d showed that ZnO-NPs have a positive surface charge of +13.0 mV.

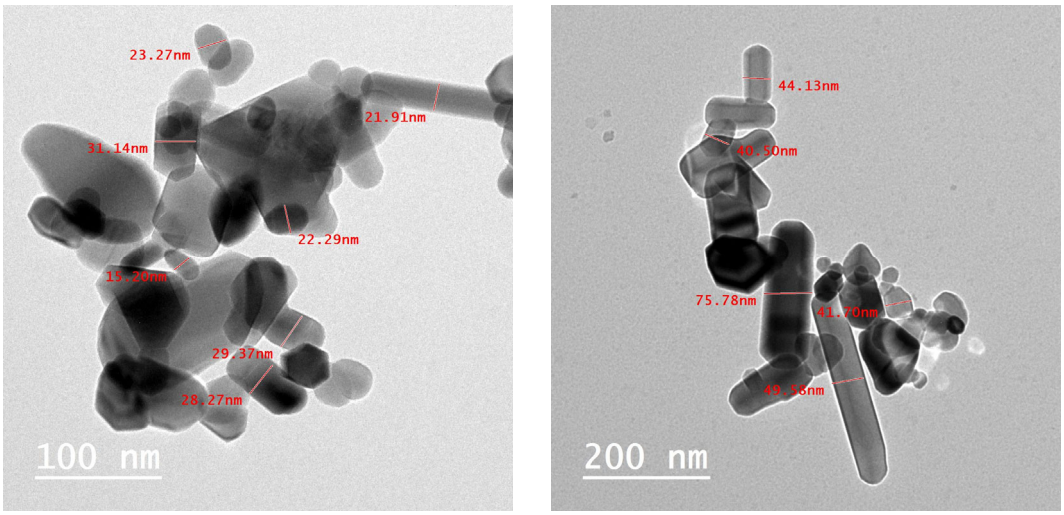

(**a**) (**b**)

Figure 4. Transmission electron microscopy images of the synthesized ZnO-NPs at scale (**a**) 100 nm and (**b**) 200 nm.

The specific surface area, pore volume, and average pore diameter of ZnO-NPs were determined by the N_2 adsorption method. Figure 5 displays an N_2 adsorption–desorption isotherm which could be classified as a Type-II isotherm. The isotherm reveals that the graph may reach a limiting value if large pores are present in high porous materials, which absorb more N_2 at low pressures. The specific surface area (S_{BET}) of ZnO-NPs is calculated to be 140.85 m^2 g^{-1} using the BET method. Furthermore, the total pore volume was 0.040 cm^3 g^{-1}, and the average pore diameter was 10.96 nm. These results confirmed the XRD and SEM findings (Figures 2b and 3). The textural properties of ZnO-NPs are listed in Table 1. Therefore, the high specific surface area and porous structure of ZnO-NP could possibly enhance its photocatalytic performance toward SERT pollutant (see below in the next sections).

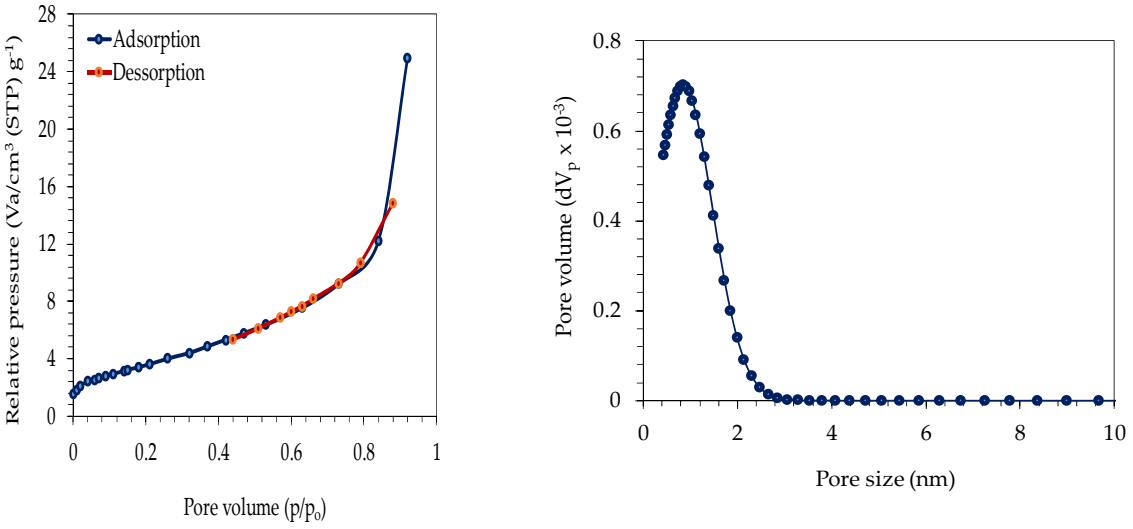

(**a**) (**b**)

Figure 5. (**a**) N_2 adsorption–desorption isotherm and (**b**) pore size distribution of the synthesized ZnO-NPs.

Table 1. The textural properties of ZnO-NPs and Bulk ZnO.

Samples' Surface Characteristics	Specific Surface Area	Average Pore Diameter	Total Pore Volume
ZnO-NP	140.85 m^2 g^{-1}	10.96 nm	0.04 cm^3 g^{-1}
ZnO-Bulk	4.83 m^2 g^{-1}	<5 micron	----

3.2. Removal of SERT by H_2O_2/UV, ZnO-NPs/H_2O_2/UV, and ZnO-NPs/UV Processes

The removal of SERT in water was performed by ZnO-NPs/UV, ZnO-NPs/H_2O_2/UV, and H_2O_2/UV processes to establish the most efficient removal process. For comparison purposes, blank experiments—UV alone, ZnO-NPs/dark, and H_2O_2/dark—were first carried out to determine the drug removal percentage by these processes. For the blank experiment conducted in the dark, in the presence of ZnO-NP only, there was 12% removal of SERT, as shown in Figure 6. Direct photolysis of SERT (UV alone) without ZnO-NP photocatalyst resulted in 7% removal of SERT concentration (see Figure 6).

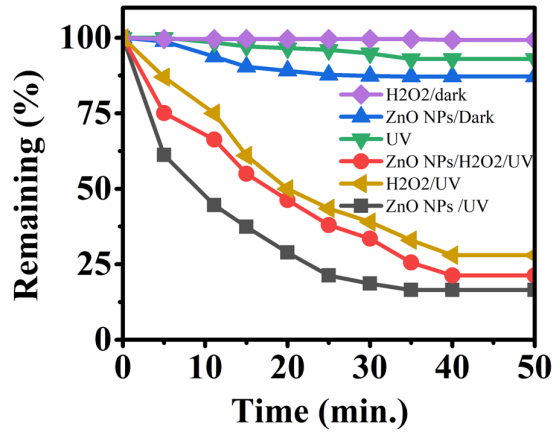

Figure 6. Removal of SERT by different processes, namely, ZnO-NPs/Dark, H_2O_2/dark, UV alone, H_2O_2/UV, ZnO-NPs/H_2O_2/UV, and ZnO-NPs/UV under the following conditions: drug concentration = 0.1 mM, catalyst dose = 0.2 g/L, natural pH (pH 7.3), T = 25 °C, and hydrogen peroxide concentration = 1 mM.

Combining ZnO-NPs and UV at the natural pH (pH 7.3) brought about significant removal of SERT in water, to 85% after 40 min of the experiment, as shown in Figure 6. This result indicated that the UV light had an evident contribution to the degradation of SERT. The photocatalytic degradation of SERT by the ZnO-NPs/UV system can be attributed to the reaction of adsorbed SERT molecules with an excited electron–hole (e^-/h^+) pair, superoxide radicals, and hydroxyl radicals and finally mineralization to CO_2 and H_2O (see below in Section 3.4), as shown in the following Equations (9)–(15) [29].

$$ZnO + h\upsilon\ (\lambda \leq 380\ nm) \rightarrow ZnO_{(e^-_{CB}+h^+_{VB})} \quad (9)$$

$$ZnO_{(e^-_{CB}+h^+_{VB})} \rightarrow Energy \quad (10)$$

$$O_2 + e^-_{CB} \rightarrow O_2^{\bullet -} \quad (11)$$

$$H_2O + h^+_{VB} \rightarrow OH^{\bullet} + H^{\bullet +} \quad (12)$$

$$O_2^{\bullet -} + h^+_{VB} \rightarrow OH^{\bullet} \quad (13)$$

$$^{\bullet}OH + \text{Drug pollutants} \rightarrow O_2 + CO_2 + H_2O \quad (14)$$

$$O_2^{\bullet -} + \text{Drug pollutants} \rightarrow CO_2 + H_2O \quad (15)$$

Using H_2O_2 alone (H_2O_2/dark) was found to have no measurable effect on drug removal (see Figure 6). However, upon UV illumination of H_2O_2, the removal of SERT shot up to 72% after 50 min, but was still less than that recorded for the ZnO-NPs/UV process, as depicted in Figure 6. The removal of SERT by the H_2O_2/UV process could be attributed to the generation of non-selective and powerful oxidant $^{\bullet}$OH radicals [30] by direct photolysis of hydrogen peroxide according to Equations (16)–(18). Hence, the efficiency of the degradation process depends mainly on the formation of hydroxyl radicals generated from the photolysis of H_2O_2. These results are in agreement with our previous work [30]. Indeed, the removal of SERT by the ZnO-NPs/H_2O_2/UV process was 75% after 40 min, which is slightly higher than that recorded for H_2O_2/UV process, by 3%, but less than that recorded for the ZnO-NPs/UV process, as shown in Figure 6. This result occurred because hydrogen peroxide can act as a scavenger for holes or $^{\bullet}$OH radicals, and, consequently, there was no enhancement in the removal of SERT by the ZnO-NPs/H_2O_2/UV process [31].

$$H_2O_2 + h\upsilon \rightarrow 2^{\bullet}OH \quad (16)$$

$$O_2^{\bullet -} + H_2O_2 \rightarrow {}^{\bullet}OH + HO^- + O_2 \quad (17)$$

$$H_2O_2 + e_{CB}^- \rightarrow {}^{\bullet}OH + HO^- \quad (18)$$

Different parameters such as pH, initial drug concentration, catalyst dose, and hydrogen peroxide concentration that can influence the photocatalytic degradation of SERT using ZnO-NPs were explored to identify the optimum conditions. Based on the results in Figure 6, we can infer that the ZnO-NPs/UV process has the highest efficiency among it and the H_2O_2/UV, and ZnO-NPs/H_2O_2/UV counterparts. This behavior can be attributed to the increased surface area and available free active sites in the case of ZnO-NPs.

3.2.1. Effect of pH

Figure 7a shows the influence of pH on the photocatalytic degradation of SERT. The results indicate better SERT removal in the alkaline region (pH 9, pH 10, and pH 11) than in the acidic region (pH 3 and pH 5) and the natural pH of SERT. Indeed, the photodegradation process of SERT in water is pH-dependent, as the highest removal was obtained at pH 11. Our findings agree with the previous studies elsewhere [32]. This behavior can be attributed to the fact that the available negative hydroxyl ions in alkaline solutions can react with a positive hole (h^+) on the catalyst surface, producing additional hydroxyl radicals of high oxidation potential, hence enhancing the degradation process [33]. On the other hand, the decrease in the degradation of SERT as the pH values change from pH 11 to pH 3 could be attributed to the high concentration of hydrogen ions, which hinders hydroxyl radical production through the reaction between hydroxyl ions and catalyst holes (h^+) [34]. Additionally, the decrease in the percentage of photodegradation with decreasing pH may be due to the dissolution of ZnO-NPs, as revealed in another study [35]. Furthermore, as the hydrogen ion concentration increases, the electrostatic repulsion between the photocatalyst ZnO-NPs surface and SERT molecules increases, decreasing the drug removal percentage [29].

Zeta potential was determined to examine the surface charges acquired by ZnO-NPs (Figure 2d) and showed that the surface is positive at the natural pH of 7.3, with a value of +13.0 mV. The pK_a value of SERT is 9.45 [36]. SERT is primarily present in the cationic ($SERT^+$) form at a natural pH of 7.3 ($pH < pk_a$). This resulted in repulsion between positively charged SERT and the positively charged ZnO-NPs. In contrast, as pH increased in an alkaline medium at pH 11, SERT presented in the non-ionized form (SERT), which decreased its repulsion with the surface of photocatalyst and consequently enhanced the photodegradation efficiency.

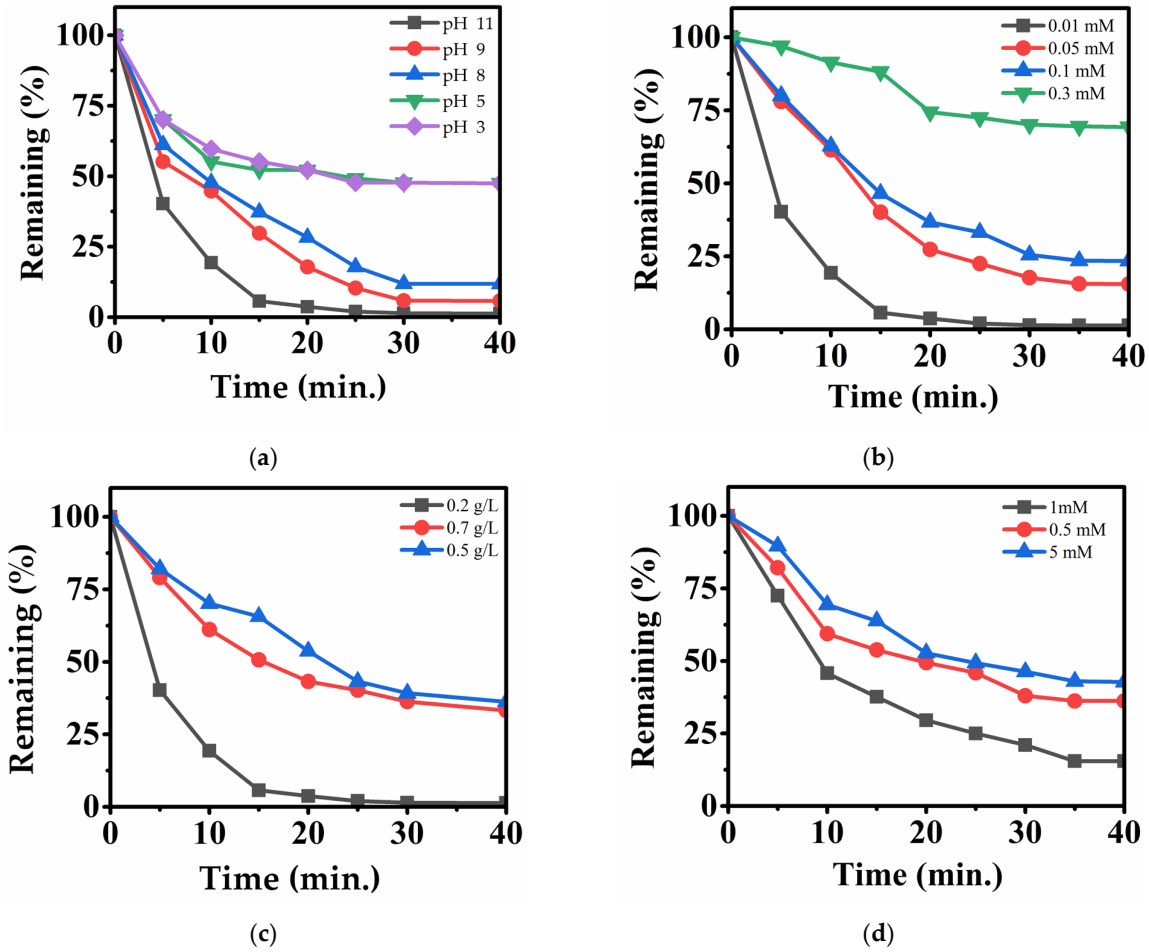

Figure 7. Effect of (**a**) pH, (**b**) initial drug concentration, (**c**) ZnO-NPs dose, and (**d**) hydrogen peroxide concentration on the removal of SERT by the ZnO-NPs/UV process at room temperature.

3.2.2. Effect of Initial Drug Concentration

The photodegradation of SERT at different initial drug concentrations (0.01, 0.05, 0.1, and 0.3 mM) in the presence of ZnO-NPs under UV illumination was investigated (at pH 11, catalyst dose = 0.2 g/L, and T 25 °C). The results given in Figure 7b reveal that the removal percentage of the drug obtained after 30 min was 98.7%, 84.5%, 76.5, and 30.1% at initial drug concentrations of 0.01, 0.05, 0.1, and 0.3 mM, respectively. These results reveal that the photodegradation of SERT decreases as the initial concentration of SERT increases. Similar results were also obtained in other studies [29,37]. This behavior could be attributed to the fact that increasing the initial drug concentration decreases the path length of the photon entering the solution, reducing the absorption [38]. As the initial drug concentration increases, the drug's adsorption on the catalyst's surface increases. This decreases the surface-active sites available for the production of hydroxyl radicals and, consequently, decreases the drug removal percentage [39]. Additionally, the increase in the initial drug concentration may decrease the absorption of UV light by the catalyst and reduce the formation of •OH radicals, which are essential in the photodegradation process, leading to a reduction of the removal percentage [40].

3.2.3. Effect of ZnO-NP Dose

Experiments were performed at different catalyst doses and kept all other parameters constant (see Figure 7c). The results indicated that, after 30 min of reaction, the removal percentage of SERT in the presence of ZnO-NPs decreased from 98.7% for 0.2 g/L to 60.8% and 63.7% for 0.5 g/L and 0.7 g/L, respectively. This behavior could be attributed to the increase in solution turbidity as the photocatalyst dose increases, thus reducing the UV

penetration [29]. Hence, the data obtained indicated that the optimum dose of ZnO-NPs was 0.2 g/L.

3.2.4. Effect of Hydrogen Peroxide

Photocatalytic degradation of SERT by ZnO-NPs in the presence of different hydrogen peroxide concentrations was investigated, and the results are shown in Figure 7d. The removal percentage of SERT was 63.8%, 98.7%, and 57.3% in the case of 0.5 mM, 1 mM, and 5 mM concentrations, respectively. The removal percentage of SERT increased as hydrogen peroxide concentration increased from 0.5 mM to 1 mM by about 35%. In contrast, a further increase in hydrogen peroxide concentration from 1 mM to 5 mM led to a decrease in the removal of the drug by about 41.5%. It is well known that, at H_2O_2 concentration greater than the critical concentration, it may act as a hole or $^{\bullet}OH$ scavenger, consequently reducing the photocatalytic activity [31]. Hence, hydrogen peroxide (with optimum concentration) increases the photodegradation rate of organic substrates [41–43].

Based on our findings, the optimum conditions for the degradation of SERT in water by the ZnO-NPs/UV process are pH 11, initial drug concentration of 0.01 mM, catalyst dose of 0.2 g/L, and reaction temperature of 25 °C.

3.2.5. Comparison of the Catalytic Activity of ZnO-NPs and Bulk ZnO in Photodegradation of SERT

The efficiency of ZnO-NPs and bulk ZnO in the presence of UV light was 98.7% and 57%, respectively, as shown in Figure 8. The results affirm that ZnO-NPs are more efficient than bulk ZnO in the removal of SERT. This behavior can be attributed to the higher surface area and more free active sites of ZnO-NPs than those of the bulk ZnO counterpart. Comparing our results with other methods reported in the literature for the removal of SERT using TiO_2/light or gamma radiation [44–46], we found the ZnO-NPs to be the most efficient photocatalyst for the removal of SERT in water within a short time.

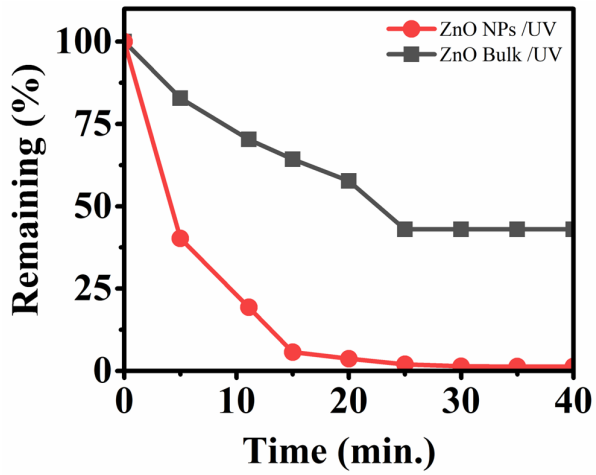

Figure 8. Photocatalytic degradation of SERT by ZnO-NPs and bulk ZnO under the following conditions: initial SERT concentration = 0.1 mM, pH = 11, catalyst dose = 0.2 g/L, hydrogen peroxide concentration = 1 mM, and T = 25 °C.

3.3. Kinetics for the Removal of SERT Using ZnO-NPs/UV

The kinetics of the photodegradation of SERT by ZnO-NPs photocatalyst was studied using zero-order, first-order, and second-order models at the optimum conditions (initial SERT concentration = 0.1 mM, pH = 11, drug dose = 0.2 g/L, and T = 25 °C). The experimental results were fitted into the chosen kinetic models and are presented in Figure 9a–c). Moreover, the chemical kinetic model of drug photodegradation was constructed using the linear regression coefficient (R^2) method, and the data are given in Table 2. As Figure 9a–c indicates, the linear regression coefficients (R^2) obtained were 0.985, 0.995, and 0.960 for

zero-order, first-order, and second-order kinetic models, respectively. These results indicate that the kinetic model of photocatalytic degradation of SERT can be represented by the first-order model with a rate constant of 0.068 min^{-1}. These results agree well with another study [47].

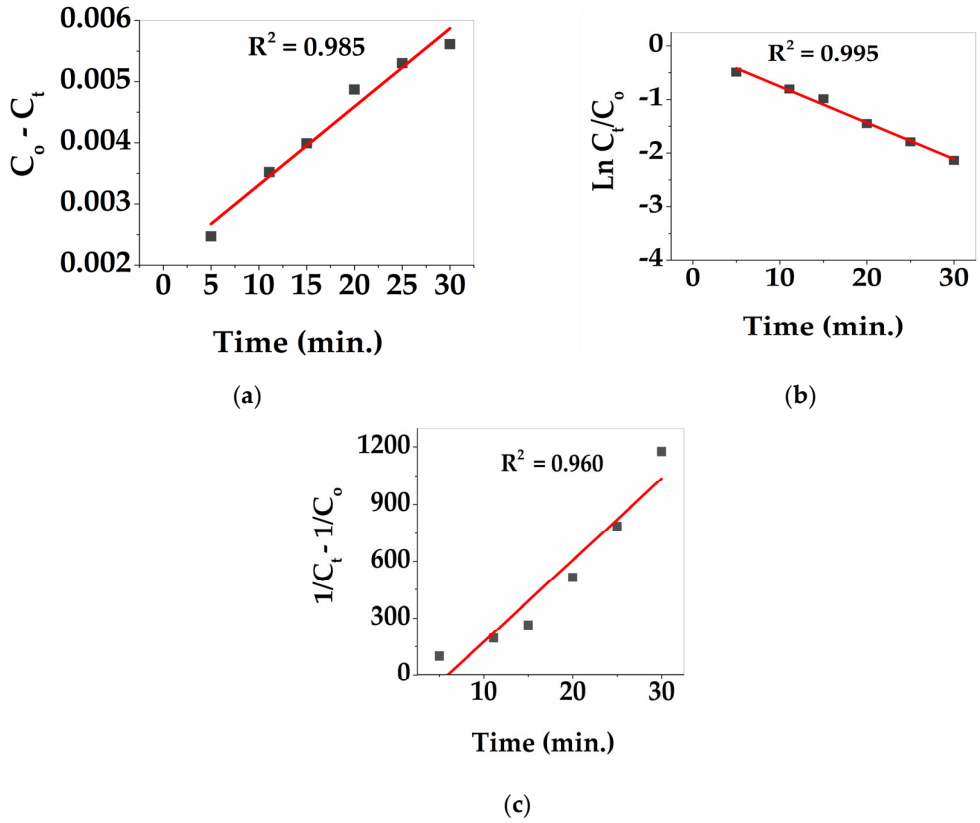

Figure 9. Linear representation of (**a**) zero-order, (**b**) first-order, and (**c**) second-order kinetics for photocatalytic degradation of SERT.

Table 2. Different kinetic models for the photocatalytic degradation of SERT by ZnO-NPs at initial SERT concentration = 0.1 mM, pH = 11, catalyst dose = 0.2 g/L, and T = 25 °C.

Kinetic Model	Regression Coefficient (R^2) Value	Rate Constant (k)
Zero-order	0.985	0.0001 min^{-1}
First-order	0.995	0.0678 min^{-1}
Second-order	0.960	43.058 min^{-1}

3.4. Mineralization of SERT by ZnO-NPs/UV and Bulk ZnO/UV Processes

Chemical oxygen demand (COD) measures the amount of oxygen required for the oxidation of organic matter present in the sample to CO_2 and water according to Equations (14) and (15). The extent of mineralization of SERT can be monitored by measuring the COD values at regular intervals [48]. A decrease in COD during photodegradation processes indicates the reduction in the carbon content in the sample, hence indicating the extent of mineralization [48]. The extent of mineralization of SERT was determined by measuring the decrease in COD values during the UV/ZnO-NPs and UV/Bulk ZnO processes (as shown in Figure 10). After 50 min of the reaction, the COD value was 74.0% for the bulk ZnO/UV process, but the highest mineralization percentage (91.1%) was achieved for the ZnO−NPs/UV process. These results reveal that the combination of UV and ZnO-NPs (UV/ZnO-NPs) proffers the most effective process for the mineralization of SERT. This behavior could be due to ZnO-NPs having a higher surface area and more active sites

than bulk ZnO. Consequently, ZnO-NPs generating more holes and hydroxyl radicals, leading to more efficient photodegradation of the drug and increasing the drug mineralization [9,10,49].

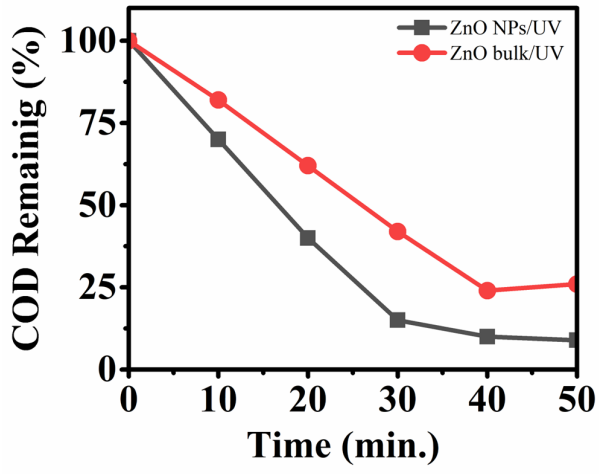

Figure 10. Change in COD values with time during photocatalytic degradation of SERT in the presence of ZnO-NPs and bulk ZnO under the following conditions: amount of bulk ZnO and ZnO-NPs = 0.2 g/L, pH = 11, hydrogen peroxide concentration = 1 mM, and T = 25 °C.

4. Conclusions

In the present contribution, we explored the photocatalytic degradation of SERT in water by different processes, namely, H_2O_2/UV, ZnO-NPs/H_2O_2/UV, and ZnO-NPs/UV. Our results indicate that SERT was successfully removed from aqueous solutions by the ZnO-NP/UV process. Nearly complete removal of SERT (98.7%) was achieved in 30 min with illuminated ZnO-NPs at room temperature. The photodegradation of SERT in water depends on the pH of the solution, initial drug concentrations, catalyst amounts, and hydrogen peroxide concentrations. Among the different processes contributing to the removal of SERT, the increasing order of the drug removal was: ZnO-NPs/UV > ZnO-NPs/H_2O_2/UV > H_2O_2/UV. Moreover, the extent of mineralization of SERT determined by measuring the COD values affirmed the ZnO-NPs/UV process to be highly efficient. The highest mineralization value was obtained for the ZnO-NPs/UV process. The results revealed that ZnO-NPs could be used effectively as a photocatalyst for the degradation and mineralization of SERT in water.

Author Contributions: Z.H.M.: conceptualization, interpretation of data for the work, methodology, formal analysis, software, and writing—review and editing. Y.M.R.: conceptualization, funding acquisition, investigation, interpretation of data for the work, writing, and review and editing. H.A.H.: conceptualization, methodology, analysis, interpretation of data for the work, validation, and review and editing. H.M.H.A.: conceptualization, interpretation of data for the work, and review and editing. All authors have read and agreed to the published version of the manuscript.

Funding: This research was funded by the Deputyship for Research & Innovation, Ministry of Education in Saudi Arabia, Research Project No. 20/5.

Data Availability Statement: Data will be made available on request.

Acknowledgments: The authors extend their appreciation to the Deputyship for Research & Innovation, Ministry of Education in Saudi Arabia for funding this research work through the project number 20/5.

Conflicts of Interest: The authors declare that they have no known competing financial interests or personal relationships that could have appeared to influence the work reported in this paper.

References

1. Kayode-Afolayan, S.D.; Ahuekwe, E.F.; Nwinyi, O.C. Impacts of pharmaceutical effluents on aquatic ecosystems. *Sci. Afr.* **2022**, *17*, e01288. [CrossRef]
2. Sörengård, M.; Campos Pereira, H.M.; Ullberg, F.Y.; Lai, O.; Golovko, A.L. Mass loads, source apportionment, and risk estimation of organic micropollutants from hospital and municipal wastewater in recipient catchments. *Chemosphere* **2019**, *234*, 931–941. [CrossRef] [PubMed]
3. Moreira, D.G.; Aires, A.; de Lourdes Pereira, M.; Oliveira, M. Levels and effects of antidepressant drugs to aquatic organisms. *Comp. Biochem. Physiol. Part C Toxicol. Pharmacol.* **2022**, *256*, 109322. [CrossRef] [PubMed]
4. Chen, Y.; Wang, J.; Xu, P.; Xiang, J.; Xu, D.; Cheng, P.; Chen, Z. Antidepressants as emerging contaminants: Occurrence in wastewater treatment plants and surface waters in Hangzhou, China. *Front. Public Health* **2022**, *10*, 963257. [CrossRef]
5. Valdez-Carrillo, M.; Abrell, L.J.; Ramírez-Hernández, J.; Reyes-López, A.; Carreón-Diazconti, C. Pharmaceuticals as emerging contaminants in the aquatic environment of Latin America: A review. *Environ. Sci. Pollut. Res.* **2020**, *27*, 44863–44891. [CrossRef] [PubMed]
6. Minagh, E.; Hernan, R.; O'Rourke, K.; Lyng, F.M.; Davoren, M. Aquatic ecotoxicity of the selective serotonin reuptake inhibitor sertraline hydrochloride in a battery of freshwater test species. *Ecotoxicol. Environ. Saf.* **2009**, *72*, 434–440. [CrossRef] [PubMed]
7. Mole, R.A.; Brooks, B.W. Global scanning of selective serotonin reuptake inhibitors: Occurrence, wastewater treatment and 440 hazards in aquatic systems. *Environ. Pollut.* **2019**, *250*, 1019–1031. [CrossRef]
8. Valdivia, M.T.; Taggart, M.A.; Pap, S.; Kean, A.; Pfleger, S.; Megson, I.L. Photocatalytic metallic nanomaterials immobilised onto porous structures: Future perspectives for pharmaceutical removal from hospital wastewater and potential benefits over existing technologies. *J. Water Process Eng.* **2023**, *52*, 103553. [CrossRef]
9. Isai, K.A.; Shrivastava, V.S. Photocatalytic degradation of methylene blue using ZnO and 2% Fe–ZnO semiconductor nanomaterials synthesized by sol–gel method: A comparative study. *SN Appl. Sci.* **2019**, *1*, 1247. [CrossRef]
10. Taourati, R.; Khaddor, M.; El Kasmi, A. Stable ZnO nanocatalysts with high photocatalytic activity for textile dye treatment. *Nano-Struct. Nano-Objects* **2019**, *18*, 100303. [CrossRef]
11. Latif, S.; Liaqat, A.; Imran, M.; Javaid, A.; Hussain, N.; Jesionowski, T.; Bilal, M. Development of zinc ferrite nanoparticles with enhanced photocatalytic performance for remediation of environmentally toxic pharmaceutical waste diclofenac sodium from wastewater. *Environ. Res.* **2023**, *216*, 114500. [CrossRef] [PubMed]
12. Krishnan, A.; Swarnalal, A.; Das, D.; Midhina, K.; Saji, V.S.; Shibli, S.M.A. A review on transition metal oxides based photocatalysts for degradation of synthetic organic pollutants. *J. Environ. Sci.* **2023**, *in press*. [CrossRef]
13. Xia, Y.; Sun, Y.; Mayers, B.; Gates, B.; Yin, Y. One-dimensional nanostructures: Synthesis, characterization, and applications. *Adv. Mater.* **2003**, *5*, 353–389. [CrossRef]
14. Mohammed, R.; Ali, M.E.M.; Gomaa, E.; Mohsen, M. Green ZnO nanorod material for dye degradation and detoxification of pharmaceutical wastes in water. *J. Environ. Chem. Eng.* **2020**, *8*, 104295. [CrossRef]
15. Samadi, M.; Zirak, M.; Naseri, A.; Kheirabadi, M.; Ebrahimi, M.; Moshfegh, A.Z. Design and tailoring of one-dimensional ZnO nanomaterials for photocatalytic degradation of organic dyes: A review. *Res. Chem. Intermed.* **2019**, *45*, 2197–2254. [CrossRef]
16. Fatima, J.; Shah, A.N.; Tahir, M.B.; Mehmood, T.; Shah, A.A.; Tanveer, T.; Nazir, R.; Jan, B.L.; Alansi, S. Tunable 2D Nanomaterials; Their Key Roles and Mechanisms in Water Purification and Monitoring, Frontiers in Environmental Science. *Front. Environ. Sci.* **2022**, *10*, 766743–766765. [CrossRef]
17. Amin, A.; Dessouki, H.; Moustafa, M.; Ghoname, M. Spectrophotometric methods for sertraline hydrochloride and/or clidinium bromide determination in bulk and pharmaceutical preparations. *Chem. Pap.* **2009**, *63*, 716–722. [CrossRef]
18. Trussell, C.G. *Standard Methods for the Examination of Water and Wastewater*; American Public Health Association: New York, NY, USA, 1989.
19. Petrović, Ž.; Ristić, M.; Musić, S.; Sepiol, B.; Peterlik, H. The formation of ZnO nanoparticles from zinc gluconate. *Ceram. Int.* **2015**, *41*, 4975–4981. [CrossRef]
20. Carvalho, A.L.F.; Freitas, D.F.S.; Mariano, D.M.; Mattos, G.C.; Mendes, L.C. The influence of zinc gluconate as an intercalating agent on the structural, thermal, morphologic, and molecular mobility of lamellar nanofiller. *Colloid Polym. Sci.* **2018**, *296*, 1079–1086. [CrossRef]
21. Shamhari, N.M.; Wee, B.S.; Chin, S.F.; Kok, K.Y. Synthesis and characterization of zinc oxide nanoparticles with small particle size distribution. *Acta Chim. Slov.* **2018**, *65*, 578–585. [CrossRef]
22. Datta, A.; Patra, C.; Bharadwaj, H.; Kaur, S.; Dimri, N.; Khajuria, R. Green Synthesis of zinc oxide nanoparticles using *Parthenium hysterophorus* leaf extract and evaluation of their antibacterial properties. *J. Biotechnol. Biomater.* **2017**, *7*, 271–276. [CrossRef]
23. Ristić, M.; Musić, S.; Ivanda, M.; Popović, S. Sol-gel synthesis and characterization of nanocrystalline ZnO powders. *J. Alloys Compd.* **2005**, *397*, L1–L4. [CrossRef]
24. Musić, S.; Dragčević, D.; Popović, S. Influence of synthesis route on the formation of ZnO particles and their morphologies. *J. Alloys Compd.* **2007**, *429*, 242–249. [CrossRef]
25. Rashidi, H.; Ahmadpour, A.; Bamoharram, F.; Zebarjad, S.M.; Heravi, M.M.; Tayari, F. Controllable one-step synthesis of ZnO nanostructures using molybdophosphoric acid. *Chem. Pap.* **2014**, *68*, 516–524. [CrossRef]
26. Ismail, M.A.; Taha, K.K.; Modwi, A.; Khezami, L. Zno Nanoparticles: Surface and X-Ray Profile Analysis. *J. Ovonic Res.* **2018**, *14*, 381–393.

27. Wang, J.; Gao, L. Synthesis and characterization of ZnO nanoparticles assembled in one-dimensional order. *Inorg. Chem. Commun.* **2007**, *6*, 877–881. [CrossRef]
28. Mohamed, K.M.; Benitto, J.J.; Vijaya, J.J.; Bououdina, M. Recent Advances in ZnO-Based Nanostructures for the Photocatalytic Degradation of Hazardous. *Non-Biodegrad. Med. Cryst.* **2023**, *13*, 329.
29. La, M.; Sharma, P.; Singh, L.; Ram, C. Photocatalytic degradation of hazardous Rhodamine B dye using sol-gel mediated ultrasonic hydrothermal synthesized of ZnO nanoparticles. *Results Eng.* **2023**, *17*, 100890.
30. Elmorsi, T.M.; Riyad, Y.M.; Mohamed, Z.H.; Abd El Bary, H.M.H. Decolorization of Mordant red 73 azo dye in water using H_2O_2/UV and photo-Fenton treatment. *J. Hazard. Mater.* **2010**, *174*, 352–358. [CrossRef]
31. Ajmal, A.; Majeed, I.; Malik, R.N.; Idriss, H.; Nadeem, M.A. Principles and mechanisms of photocatalytic dye degradation on TiO_2 based photocatalysts: A comparative overview. *RSC Adv.* **2014**, *4*, 37003–37026. [CrossRef]
32. Giacco, D.; Tiziana, R.G.; Saracino, F.; Stradiotto, M. Counterion effect of cationic surfactants on the oxidative degradation of Alizarin Red-S photocatalysed by TiO_2 in aqueous dispersion. *J. Photochem. Photobiol.* **2017**, *332*, 546–553. [CrossRef]
33. Hariharan, C. Photocatalytic degradation of organic contaminants in water by ZnO nanoparticles: Revisited. *Appl. Catal. A Gen.* **2006**, *304*, 55–61. [CrossRef]
34. El-Kemary, M.; El-Shamy, H.; El-Mehasseb, I. Photocatalytic degradation of ciprofloxacin drug in water using ZnO nanoparticles. *J. Lumin.* **2010**, *130*, 2327–2331. [CrossRef]
35. Muruganandham, M.; Swaminathan, M. Photocatalytic decolorizations and degradation of Reactive Orange 4 by TiO_2-UV process. *Dyes Pigm.* **2006**, *68*, 133–142. [CrossRef]
36. Deák, K.; Takács-Novák, K.; Tihanyi, K.; Noszá, B. Physico-Chemical Profiling of Antidepressive Sertraline: Solubility, Ionisation, Lipophilicity. *Med. Chem.* **2006**, *2*, 385–389.
37. Akyol, A.; Yatmaz, H.C.; Bayramoglu, M. Photocatalytic decolorization of Remazol Red RR in aqueous ZnO suspensions. *Appl. Catal. B Environ.* **2004**, *54*, 19–24. [CrossRef]
38. Krishnakumar, B.; Swaminathan, M. Influence of operational parameters on photocatalytic degradation of a genotoxic azo dyeAcid Violet 7 in aqueous ZnO suspensions. *Spectrochim. Acta Part A Mol. Biomol. Spectrosc.* **2011**, *81*, 739–744. [CrossRef]
39. Jiang, Y.; Sun, Y.; Liu, H.; Zhu, F.; Yin, H. Solar photocatalytic decolorization of C.I. Basic Blue 41 in an aqueous suspension of TiO_2-ZnO. *Dyes Pigm.* **2008**, *78*, 77–83. [CrossRef]
40. Nguyen, C.H.; Fu, C.C.; Juang, R.S. Degradation of methylene blue and methyl orange by palladium-doped TiO_2 photocatalysis for water reuse: Efficiency and degradation pathways. *J. Clean. Prod.* **2018**, *202*, 413–427. [CrossRef]
41. Lee, K.M.; Lai, C.W.; Ngai, K.S.; Juan, J.C. Recent developments of zinc oxide based photocatalyst in water treatment technology: A review. *Water Res.* **2016**, *88*, 428–448. [CrossRef]
42. Zuorro, A.; Lavecchia, R.; Monaco, M.M.; Iervolino, G.; Vaiano, V. Photocatalytic Degradation of azo dye reactive violet 5 on Fe-doped titania catalysts under visible light irradiation. *Catalysts* **2019**, *9*, 645. [CrossRef]
43. Al-Mamun, M.R.; Kader, S.; Islam, M.S. Solar-TiO_2 immobilized photocatalytic reactors performance assessment in the degradation of methyl orange dye in aqueous solution. *Environ. Nanotechnol. Monit. Manag.* **2021**, *16*, 100514. [CrossRef]
44. Rejek, M.; Grzechulska-Damszel, J. Degradation of sertraline in water by suspended and supported TiO_2. *Pol. J. Chem. Technol.* **2018**, *20*, 107–112. [CrossRef]
45. Calza, P.; Jiménez-Holgado, C.; Coha, M.; Chrimatopoulos, C.; Dal Bello, F.; Medana, C.; Sakkas, V. Study of the photoinduced transformations of sertraline in aqueous media. *Sci. Total Environ.* **2021**, *756*, 143805. [CrossRef] [PubMed]
46. Bojanowska-Czajka, A.; Pyszynska, M.; Majkowska-Pilip, A.; Wawrowicz, K. Degradation of selected antidepressants sertraline and citalopram in ultrapure water and surface water using gamma radiation. *Processes* **2021**, *10*, 63. [CrossRef]
47. Alamier, W.M.; Hasan, N.; Ali, S.K.; Oteef, M.D.Y. Biosynthesis of Ag nanoparticles using carallumaacutangula extract and its catalytic functionality towards degradation of hazardous dye pollutants. *Crystals* **2022**, *12*, 1069. [CrossRef]
48. Pera, S.P.; Tank, S.K. Microbial degradation of Procion Red by *Pseudomonas stutzeri*. *Sci. Rep.* **2021**, *11*, 3075.
49. Brillas, E.; Sirés, I. Electrochemical removal of pharmaceuticals from water streams: Reactivity elucidation by mass spectrometry. *Trends Anal. Chem.* **2015**, *70*, 112–121. [CrossRef]